Electron paramagnetic resonance of Fe^{3+} in near-stoichiometric $LiTaO_3$

2004 J. Phys.: Condens. Matter 16 9047

(http://iopscience.iop.org/0953-8984/16/49/020)

INSTITUTE OF PHYSICS PUBLISHING JOURNAL OF PHYSICS: CONDENSED MATTER

J. Phys.: Condens. Matter **16** (2004) 9047–9057 PII: S0953-8984(04)86998-4

Electron paramagnetic resonance of Fe^{3+} in near-stoichiometric $LiTaO_3$

M Loyo-Menoyo[1], D J Keeble[1], Y Furukawa[2] and K Kitamura[3]

[1] Carnegie Laboratory of Physics, Faculty of Engineering and Physical Sciences, University of Dundee, Dundee DD1 4HN, UK
[2] Oxide Corporation, Kobuchi-sawa, Yamanashi 408-004, Japan
[3] National Institute for Materials Science, Tsukuba 305-0044, Japan

E-mail: d.j.keeble@dundee.ac.uk

Received 30 September 2004, in final form 3 November 2004
Published 26 November 2004
Online at stacks.iop.org/JPhysCM/16/9047
doi:10.1088/0953-8984/16/49/020

Abstract

Electron paramagnetic resonance (EPR) experiments on the dominant Fe^{3+} centre in near-stoichiometric $LiTaO_3$ crystals grown by the double crucible Czochralski method are reported. A near complete roadmap of EPR positions was obtained, and transitions from two magnetically non-equivalent sites clearly resolved in the *zx* plane, perpendicular to the glide plane. This allowed accurate determination of C_3 symmetry spin Hamiltonian parameters. Newman superposition model analyses of second and fourth order zero field splitting term parameters were performed to give further insight into the site of incorporation. The second order calculations provide evidence for Fe^{3+} substitution within the Li octahedron.

1. Introduction

Lithium tantalate is an attractive optoelectronic ferroelectric material due to its favourable non-linear optical properties and a large electro-optic effect. Recently efficient second harmonic generation of blue and red light has been obtained from a periodically poled crystal [1]. It has also been used to fabricate an optical multichannel correlator, based on the photorefractive effect [2]. Iron doped $LiTaO_3$ gives an large photorefractive effect that has been successfully used for non-volatile holographic storage [3]. To gain insight into the microscopic mechanisms it is necessary to determine to local environment of the incorporated impurity ion.

Advances in crystal growth have allowed near-stoichiometric $LiTaO_3$ to be grown, in contrast to the commonly available lithium deficient congruent material ($Li/[Li + Ta] \sim 0.485$) [4]. Conventionally grown crystals are expected to contain considerable concentrations of either or both Li vacancies and Ta antisite defects. Lithium tantalate has a single structural phase transition from a high temperature paraelectric phase

to a ferroelectric phase. This has been commonly reported to be at 620 °C; however, recent measurements on near-stoichiometric crystals give a value of 685 °C [4].

Two experimental studies have been reported that give local structure information on the incorporation of Fe^{3+} in $LiTaO_3$. Electron nuclear double resonance (ENDOR) has provided good evidence that Fe^{3+} incorporates at the Li site [5]. The study was performed on a congruent crystal and reported large linewidths, consistent with the presence of near neighbour defects. Subsequently, extended x-ray absorption fine structure (EXAFS) measurements on high Fe concentration (9%) $LiTaO_3$ powders were made, and they supported the assignment of Fe^{3+} substituting at the Li site [6].

Electron magnetic resonance (EMR) provides sensitive techniques for studying Fe^{3+} ions that can often give detailed insight on the local site. The spectra can be analysed in terms of a spin-Hamiltonian (SH) of the form

$$\hat{\mathbf{H}} = \beta_e \mathbf{B} \cdot \mathbf{g} \cdot \hat{\mathbf{S}} + \hat{\mathbf{H}}_{\mathrm{ZFS}} + \sum_i (\hat{\mathbf{I}}_i \cdot \mathbf{A}_i \cdot \hat{\mathbf{S}} - g_{n,i} \beta_n \mathbf{B} \cdot \hat{\mathbf{I}}_i) \tag{1}$$

containing electronic Zeeman, zero field splitting (ZFS), nuclear hyperfine, and nuclear Zeeman terms, with the sum including all relevant neighbour magnetic nuclei. Only the first two terms are required for a description of Fe^{3+} electron paramagnetic resonance (EPR) in $LiTaO_3$; all are required for an analysis of ENDOR experiments. The ZFS terms can be expressed using Stevens spin operators,

$$\hat{\mathbf{H}}_{\mathrm{ZFS}} = \sum_{k=2,4} \sum_{q=-k}^{k} B_k^q \hat{\mathbf{O}}_k^q(S_x, S_y, S_z) = \sum_{k=2,4} \sum_{q=-k}^{k} f_k b_k^q \hat{\mathbf{O}}_k^q(S_x, S_y, S_z) \tag{2}$$

where the relevant scaling factors are $f_2 = 1/3$ and $f_4 = 1/60$ and the explicit form of the spin operators are listed elsewhere [7]. The spin and site symmetry of the paramagnetic centre dictate which SH terms are non-zero. For $S = \frac{5}{2}$ centres only terms $k = 2, 4$, with $-k \leqslant q \leqslant k$, are allowed. The Laue class of the point group imposes further constraints [8]. The two trigonal classes are relevant here; both can result in non-zero b_2^0, b_4^0, b_4^{-3}, and b_4^3 ZFS parameters. The later two are termed the trigonal fourth order terms, and they transform with rotation of the xy axes by an angle ϕ about the C_3 axis according to the expression

$$[b_k^q] = \sin(q\phi)\{b_k^{-q}\} + \cos(q\phi)\{b_k^q\}. \tag{3}$$

For C_{3v}, if the experimental y axis is defined to be coincident with a twofold rotation axis, then b_4^3 is the only non-zero trigonal term.

Ferroelectric $LiTaO_3$ is described by the $R3c$ space group [9–11]; in the paraelectric phase this becomes $R\bar{3}c$. The ferroelectric structure is a member of the ilmenite group of trigonal simple titanium oxides that retain ABO_3 perovskite blocks. It is commonly described by a hexagonal unit cell containing six formula units. There is a sequence of distorted octahedra, joined by their faces along a trigonal polar c axis, and filled in the sequence Li, Ta, vacancy. Pairs of similar C_3 sites are related by $c/2$ glide operations; see figure 1. The three equivalent hexagonal a axes are, by convention, defined to be perpendicular to the glide planes. The standard orientation of the x, y, and z principal axes, used to describe the physical properties, sets the z axis parallel to the hexagonal c axis and the x axis parallel to an a axis [12]. In this convention the glide plane is the zy plane. The point group for the octahedral sites is reduced from C_{3v} to C_3 by the slight twisting of the two trigonal oxygen atom planes with respect to each other. This is clearly seen in figure 1 and is quantified in table 1 by the angle α. Below the transition temperature both cations (Li^{1+} and Ta^{5+}) are displaced along the c axis away from the octahedron centres and a significant polarization, $\sim 50\ \mu\mathrm{C\ cm^{-2}}$, results.

Two reports on the EPR spin-Hamiltonian parameters for Fe^{3+} in $LiTaO_3$ have been made [5, 13]. The initial EMR study determined the magnitude of the axial second order ZFS

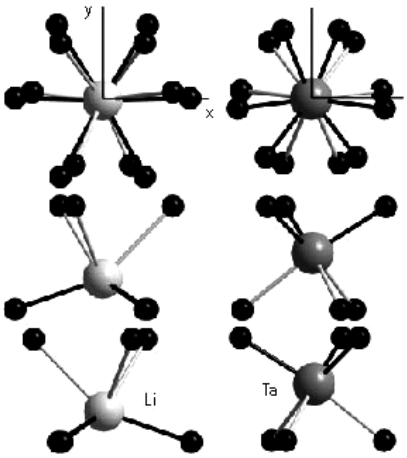

Figure 1. Comparison of symmetry related Li and Ta sites (middle and bottom). Projection on the xy plane (top).

Table 1. Structural parameters for Li and Ta sites in $LiTaO_3$. The data are from the inorganic crystal structure database (ICSD). Polar coordinates are given with respect to conventional Cartesian axes. The azimuthal angle to the first upper oxygen is ϕ_1, the similar angle for the lower triangle is ϕ_2.

Ref./ICSD	[9]/9537	[10]/84226	[11]/84579
c (nm)	1.378 35	1.378 06(5)	1.3783(3)
a (pm)	515.428(1)	515.329(7)	515.4(3)
2α (Li site) (deg)	8.46	7.76	7.75
R_1 (Li–O) (pm)	229.36	225.86	230.70
θ_1 (Li–O) (deg)	43.49	44.28	43.04
ϕ_1 (deg)	7.66	6.55	6.43
R_2 (Li–O) (pm)	207.63	206.48	204.12
θ_2 (Li–O) (deg)	107.75	109.23	107.42
ϕ_2 (deg)	59.19	58.80	58.68
2α (Ta site) (deg)	1.04	1.13	1.24
R_1 (Ta–O) (pm)	189.09	194.82	190.99
θ_1 (Ta–O) (deg)	59.56	58.01	60.18
ϕ_1 (deg)	111.59	112.32	112.34
R_2 (Ta–O) (pm)	207.00	202.13	207.24
θ_2 (Ta–O) (deg)	130.31	128.73	130.56
ϕ_2 (deg)	52.34	53.44	53.58

term, $b_2^0/h = 9.9(1)$ GHz, which describes the main features of the EPR spectrum [5]. The large linewidths and asymmetric lineshapes, characteristic of non-stoichiometric crystals [14], were observed. Subsequently two theoretical studies [15, 16] attempted to derive local structure information from an analysis of the experimental b_2^0 value. Zheng [15] used both a microscopic mechanism and a Newman superposition model (SPM) [17, 18] analysis and concluded that Fe^{3+} was displaced 24(11) pm from the Li site, away from the centre of the octahedron. Yeom [16] used an SPM analysis to calculate both second and fourth order ZFS terms and found good agreement with experiment for b_2^0 assuming Fe^{3+} substituted at the Li site; no experimental fourth order experimental values were available for comparison.

Recently Vazhenin *et al* [13] reported a study of Fe^{3+} in a congruent single crystal subjected to prolonged high temperature annealing in the appropriate LiO_2 vapour pressure to produce

Table 2. Reported spin-Hamiltonian parameters for the Fe^{3+} centre in $LiTaO_3$.

$g_\parallel$	$g_\perp$	(b_2^0/h) (GHz)	(b_4^0/h) (GHz)	$(\lvert b_4^3\rvert/h)$ (GHz)	(b_4^{-3}/h) (GHz)	$(\lvert v_4^3\rvert/h)$ (GHz)	T (K)	Reference
1.995(2)	1.995(2)	9.9(1)					15	[5]
2.001(1)	1.998(15)	9.60(2)	0.005(5)	4.180(25)		4.18	305	[13]

near-stoichiometric material. Symmetric lines and a linewidth for B parallel to the c axis of approximately 2 mT were observed. A partial roadmap of EPR lines in the zx plane is given and both second and fourth order ZFS terms derived; see table 2. The presence of the glide plane in the $LiTaO_3$ structure requires that a paramagnetic centre substituted at one of the axial sites has a structurally equivalent site related by the axial glide operation; see figure 1. The reflection operation results in the non-equivalence of the SHs for the centres in the two sets of sites [19]. The parameter g_{xy} transforms to $-g_{yx}$ and b_4^3 to $-b_4^3$. A consequence is that certain transitions observed as singlets in the glide plane, the zy plane, are expected to split into doublets in the zx plane. This was observed by Vazhenin *et al* [13] for the one of the loop transitions.

Here detailed EPR measurements are reported from as-grown near-stoichiometric $LiTaO_3$ single crystals; high field transitions and all symmetry split transitions are clearly resolved, allowing accurate spin-Hamiltonian parameters to be determined. Superposition model analyses of both the second and fourth order zero field splitting terms using the available crystals structures are presented and discussed.

2. Experimental method

Two near-stoichiometric crystals, grown using a double crucible Czochralski method from an Li rich (about 60 Li_2O mol%) melt composition, were studied. Both were $3 \times 3 \times 8$ mm^3, an x-cut (major axis along [100]) and a z-cut (major axis along [001]); the former was subsequently divided for measurements in the zx plane. The crystals were not intentionally doped. In addition an x- and z-cut pair of non-stoichiometric crystals were studied. EPR measurements in the region of 9.5 GHz were performed using a Bruker EMX spectrometer. The microwave frequency was measured and two magnet systems were used, one with a maximum field, B_{max}, of 0.9 T, the other with $B_{max} = 2.1$ T. The magnetic field of the 0.9 T system was monitored using an NMR magnetometer. The samples were mounted on an automated goniometer with precision of $\pm 0.125°$. Variable temperature measurements were taken using an Oxford Instruments ESR900 cryostat. EPR spectral simulations were performed by exact diagonalization of the appropriate spin-Hamiltonian using the computer program EPR-NMR [20].

3. EPR results

The room temperature EPR line positions measurements in both the zy and zx planes, due to the Fe^{3+} centre, are shown in figure 2. In addition, transitions due to Cr^{3+} were identified but are not shown. The lineshapes were symmetric and the linewidth varied from $\sim$2 mT for B parallel to c to $\sim$4 mT for other angles. A non-stoichiometric crystal was also studied; this showed asymmetric lineshapes with linewidths that varied from $\sim$2 mT for B parallel to c but to $\sim$12 mT for other angles.

The main features of the roadmap were fitted by adjusting the value of b_2^0; fitting of the parallel and perpendicular high field line positions provided an accurate value. Lines from

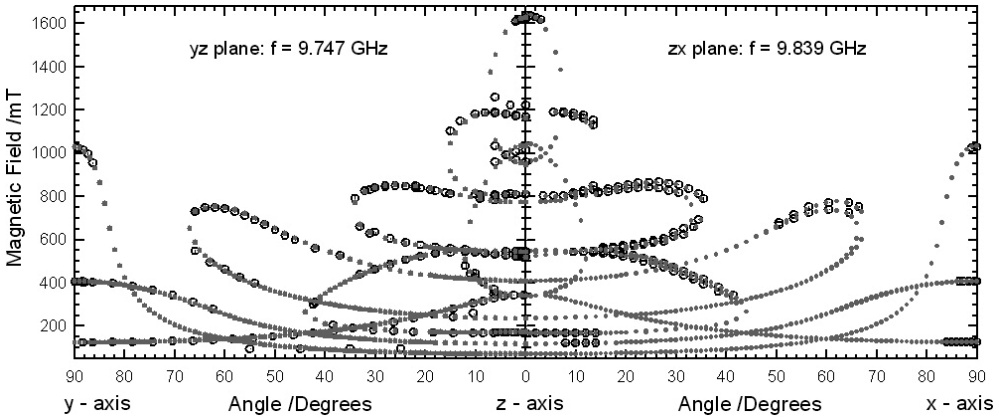

Figure 2. Experimental EPR line positions (black open circles) and line positions simulated using the spin-Hamiltonian parameters given in table 3 (grey solid circles).

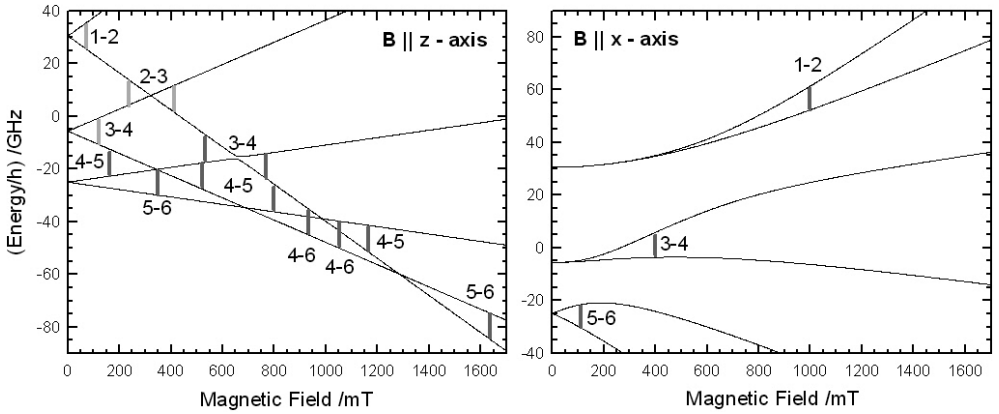

Figure 3. Energy level diagrams for magnetic field parallel to z and x axes with EPR transitions marked.

the two inequivalent sites, with sign reversed b_4^3 term values, are clearly resolved in the zx plane. An accurate magnitude for b_4^3 was determined by fitting these splittings. A number of transitions are sensitive to the fourth order terms and an iterative process allowed values to be obtained for all terms. Comparisons of line intensities for transitions 5–6 and 1–2 for B perpendicular to z, see figure 3, were carried out between room temperature and 10 K and gave a positive sign for b_2^0. The resulting SH parameters values are given in table 3, and the line position is shown in figure 2. The energy level diagrams for the magnetic field directions parallel to the z and x axes are shown in figure 3, and the EPR transitions are marked. Figure 4 shows the portion of the energy level diagram for 32° in the zx plane where the two sets of levels, resulting from the sign reversed b_4^3 sites, give doublets.

The temperature dependence of the SH parameters was determined though the range 10–300 K and the results are shown in figure 5. An approximately linear behaviour is observed for the second order term, $(b_2^0/h)(T) = (9.765(12)–0.001\,87(8)T)$ GHz. The temperature dependence of b_4^0 is also shown; the values of $|b_4^3|$ and b_4^{-3} were found to be constant within error. The temperature dependence of b_4^0 showed a minimum magnitude in the region of 150 K.

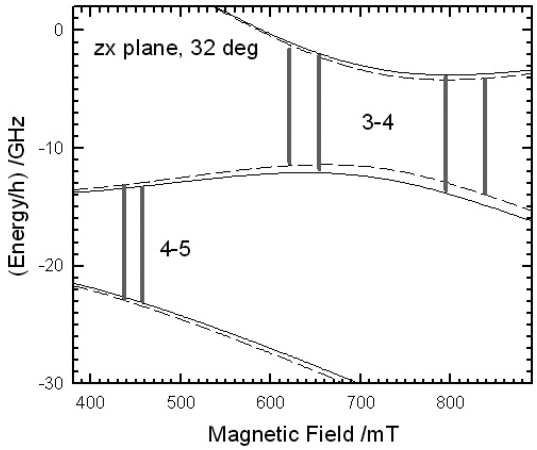

Figure 4. Energy level diagram for the magnetic field direction of 32° in the zx plane. Levels calculated with $+b_4^3$ (solid curve) and $-b_4^3$ (dashed curve) are shown along with observed EPR transitions.

Table 3. Measured room temperature spin-Hamiltonian parameters for Fe^{3+} in $LiTaO_3$.

$g_\parallel$	$g_\perp$	(b_2^0/h) (GHz)	(b_4^0/h) (GHz)	$(\lvert b_4^3\rvert/h)$ (GHz)	(b_4^{-3}/h) (GHz)	$(\lvert v_4^3\rvert/h)$ (GHz)
2.012(3)	2.000(2)	+9.22(2)	−0.18(3)	3.6(6)	−0.48(40)	3.6

Table 4. Relevant superposition model coordination factors.

K_2^0	$\frac{1}{2}(3\cos^2\theta - 1)$
K_4^0	$\frac{1}{8}(35\cos^4\theta - 30\cos^2\theta + 3)$
K_4^3	$35\sin^3\theta\cos\theta\cos 3\phi$
K_4^{-3}	$35\sin^3\theta\cos\theta\sin 3\phi$

4. Superposition model analysis

The Newman superposition model (SPM) analysis allows the SH ZFS values to be calculated from a structural model for the nearest neighbour ligand ions [17, 18]. The ZFS terms are assumed to result from the sum of contributions from only these ions. Each is assumed to be axially symmetric with respect to the line joining it to the paramagnetic ion and can be described by an intrinsic parameter function, $\bar{b}_k(R_L)$. The relevant ZFS term can then be calculated using the expression

$$b_k^q = \sum_L \bar{b}_k(R_L) K_{kq}(\theta_L, \phi_L). \tag{4}$$

$K_{kq}(\theta_L, \phi_L)$ are relevant geometric factors; see table 4. The intrinsic functions are derived from experiments on model cubic materials, for example MgO and CaO, and are obtained in the form of a power law (PL) relation defined about a reference distance, R_0, characteristic of the model material used,

$$\bar{b}_K(R_L) = \bar{b}_k(R_0)\left(\frac{R_0}{R}\right)^{t_k}. \tag{5}$$

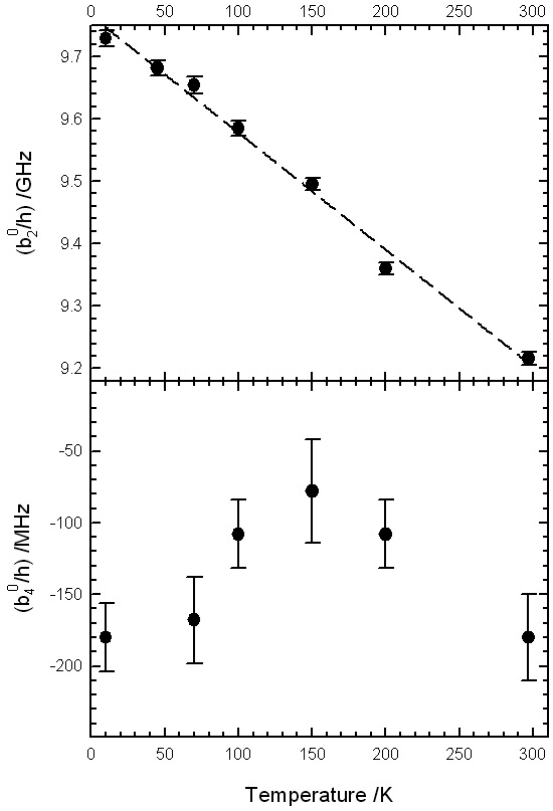

Figure 5. Temperature dependence of ZFS terms b_2^0 and b_4^0.

Table 5. Superposition model parameter values for Fe^{3+} with O^{2-} ligands.

Host	R_0 (pm)	$\bar{b}_2/h$ (GHz)	t_2	Reference	$\bar{b}_4/h$ (MHz)	Reference
CaO	239.8	−6.75 (60)	5(1)	[21]	27.3(1)	[28]
MgO	210.1	−12.35 (75)	8(1)	[21]	87.8(1.4)	[21]
$SrTiO_3$	195.2	−20(3)	8(1)	[21]	84.9(1.4)	[29]
	200.0	−4.65(14)	16	[24]	29.7(2.4)	[24]

Newman and Siegel [21] analysed stress dependent EPR experiments for Fe^{3+} in MgO and CaO and provided values for PL parameters. These were reproduced by Siegel and Müller [22] and values for $SrTiO_3$ added; see table 5. More generally it is assumed that $\bar{b}_k(R_L)$ contains both positive and negative contributions and that a Lennard-Jones (LJ) type expression should provide a more accurate description, particularly for larger deviations of R_L from R_0 [17, 23]. Care must be taken applying (5) where values of R_L are significantly smaller than R_0.

Determinations of the PL parameters are subject to two main error sources. It is normally assumed that the ion–ligand distance R_0 is the same as the host lattice value; however, substitution of the paramagnetic ion can result in local relaxation due to charge imbalance and size misfit. Secondly, any deviation in the local elastic stiffness constants from their bulk values will cause a change in the derived intrinsic parameters. Yeung [24] and Agulló-López and Müller [25] have attempted to correct the SPM intrinsic parameter values.

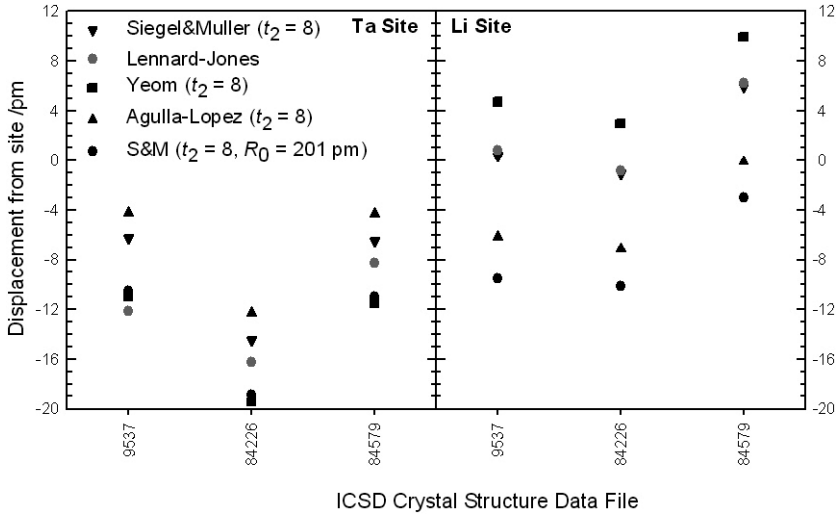

Figure 6. Superposition model results for b_2^0 using the crystal structures detailed in table 1. The displacement from the host lattice site for which the calculated value is in agreement with experiment is shown. The methods of calculation are discussed in the text.

Calculations were performed using the available crystal structures detailed in table 1. Calculations of b_2^0 were made using the intrinsic parameters listed in table 5; in addition, the Lennard-Jones expression for Fe^{3+} in MgO and the calculation methods of Agulló-López and Müller [25] and Yeom [26] were used. For the relevant parameter sets and methods, calculations were made using the t_2 values 7 and 8. Analysis was also performed using the conventional MgO parameter values, see table 5, but with the experimental R_0 of 201 pm obtained from EXAFS [27]. A representative selection of the results is shown in figure 6. The ion was free to displace along C_3 axis to a position where the calculated and experimental values were in agreement. Displacement of the Fe^{3+} towards the centre of the Li octahedron was, on average, required for agreement. At the Ta site a displacement away from the centre was needed.

Calculations of the fourth order terms were also made using the three crystal structures and the parameter values given in table 5; the t_4 values used were 12, 14, and 16. A representative selection of the results for the fourth order parameter values, calculated assuming substitution exactly on-site, are shown in figure 7. The variation in calculated parameter value with displacement off-site is illustrated in figure 8 using the crystal structure of Hsu *et al* [11].

5. Discussion

The observation of a near complete roadmap of EPR transitions in the zy and zx planes, and the presence of several clearly resolved symmetry related splittings, has allowed the spin-Hamiltonian parameters to be accurately determined. The dominant second order axial ZFS term value is in approximate agreement with the two previous studies; see tables 2 and 3. The slightly higher values reported earlier can likely be explained by the omission of a sufficiently large negative fourth order axial term. The order of magnitude of the fourth order trigonal terms, $|v_4^3| = \{(b_4^3)^2 + (b_4^{-3})^2\}^{\frac{1}{2}}$, reported here is comparable to that given by Vazhenin *et al* [13]. It was found that a finite b_4^{-3} term was required for the best fit to the experimental roadmap, consistent with the expected C_3 symmetry for Fe^{3+} in $LiTaO_3$.

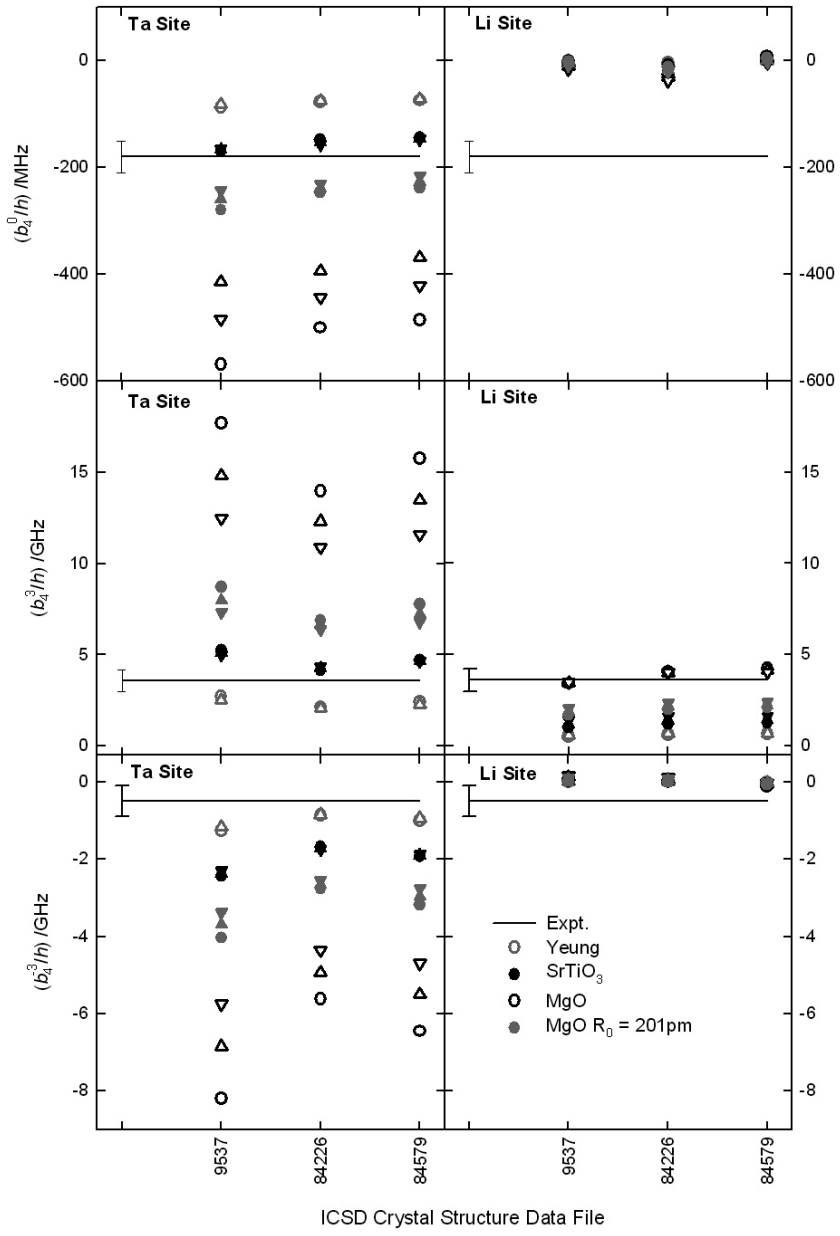

Figure 7. Superposition model results for the fourth order ZFS terms using the crystal structures detailed in table 1 assuming substitution exactly at either the Li or Ta sites. The calculations are repeated for different methods (see table 5) and exponent values, $t_4 = 16$ (circle), 14 (triangle-up), 12 (triangle-down).

Despite the limitations of the superposition model, it provides a useful framework for discussing the local environment of the paramagnetic ion. The calculations of b_2^0 given in figure 6 show that, on average, to obtain agreement with experiment the Fe^{3+} ion must be displaced off the Ta site away from the centre of the oxygen octahedron. Substitution within

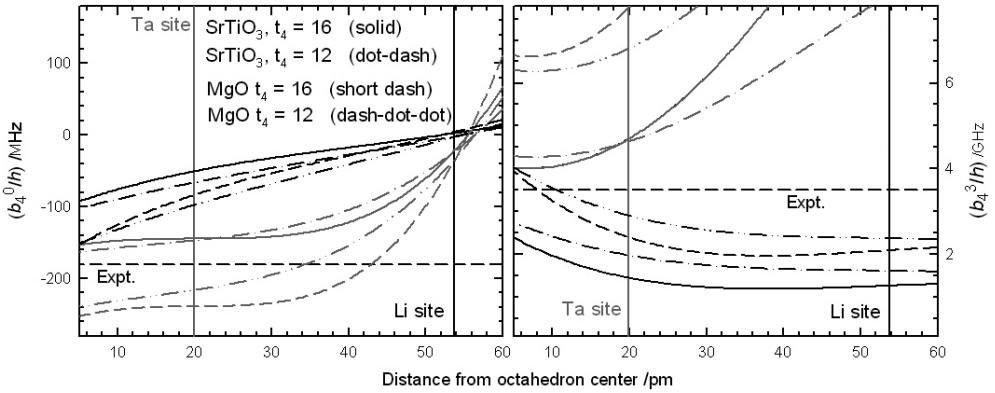

Figure 8. Superposition model fourth order ZFS term calculations as a function of displacement from the centre of either the Li (black) or Ta (grey) octahedron. The results for two SPM methods, MgO with $R_0 = 201$ pm and $SrTiO_3$ (see table 5), using the crystal structure from REF [11] are shown.

the Li octahedron gives a similar spread of results but centred about the Li site position. The results tend to support the conclusion of previous work [5, 6, 16] that Fe^{3+} substitutes near the Li site.

The fourth order SPM calculations could not provide simultaneous agreement, for a given parameter set and displacement, with the second order calculation for all the ZFS terms. The shorter radial distances to the oxygen ions at the Ta site make these calculations more sensitive to the parameter set and method used. The narrower spread of fourth order values at the Li site, see figure 7, are in approximate agreement with the experimental values, apart from b_4^0 which is consistently underestimated. The wide variation in calculated values at the Ta site spans the experiment, but for a given intrinsic parameter set there is no simultaneous agreement for all the fourth order terms; see figure 7. Further, as noted earlier, the second order calculations within the Ta octahedron require an off-site displacement away from the centre.

The SPM calculations assume an un-relaxed oxygen ion geometry, and allow only the Fe^{3+} ion to displace; otherwise, too many degrees of freedom result. However, the EXAFS results provide evidence for a contraction of the Fe^{3+} oxygen distances [6].

6. Conclusions

The significantly narrower Fe^{3+} EPR linewidths observed for near-stoichiometric, compared to non-stoichiometric, $LiTaO_3$ crystals has allowed line splittings in the plane perpendicular to the glide plane to be clearly resolved. These contribute to the determination of an accurate spin-Hamiltonian fit consistent with C_3 symmetry, see table 3, confirming that Fe^{3+} ions substitute at sites on the trigonal axis. Superposition model calculations of the dominant axial second order zero field splitting term provide evidence supporting the model of Fe^{3+} substituting within the Li octahedron.

Acknowledgments

DJK wishes to acknowledge support from Carnegie Research Grants for this work; MLM was supported by an EPSRC quota studentship.

References

[1] Luo G Z, Zhu S N, He J L, Zhu Y Y, Wang H T, Liu Z W, Zhang C and Ming N B 2001 *Appl. Phys. Lett.* **78** 3006
[2] Ryf R, Montemezzani G, Gunter P, Furukawa Y and Kitamura K 2001 *Appl. Phys.* B **72** 737
[3] Imbrock J, Kip D and Kratzig E 1999 *Opt. Lett.* **24** 1302
[4] Furukawa Y, Kitamura K, Suzuki E and Niwa K 1999 *J. Cryst. Growth* **197** 889
[5] Sothe H, Rowan L G and Spaeth J M 1989 *J. Phys.: Condens. Matter* **1** 3591
[6] Catlow C R A, Chadwick A V, Cole M and Tomlinson S M 1991 *Radiat. Eff. Defects Solids* **119** 565
[7] Abragam A and Bleaney B 1970 *Electron Paramagnetic Resonance of Transition Ions* (Oxford: Clarendon)
[8] McGavin D G 1987 *J. Magn. Reson.* **74** 19
[9] Abrahams S C and Bernstein J L 1967 *J. Phys. Chem. Solids* **28** 1685
[10] Ohgaki M, Tanaka K and Marumo F 1989 *Mineral. J.* **14** 373
[11] Hsu R, Maslen E N, duBoulay D and Ishizawa N 1997 *Acta Crystallogr.* B **53** 420
[12] Weis R S and Gaylord T K 1985 *Appl. Phys.* A **37** 191
[13] Vazhenin V A, Guseva V B, Artyomov M Y, Route R K, Fejer M M and Byer R L 2003 *J. Phys.: Condens. Matter* **15** 275
[14] Malovichko G, Grachev V and Schirmer O 1999 *Appl. Phys.* B **68** 785
[15] Zheng W C 1998 *Radiat. Eff. Defects Solids* **145** 329
[16] Yeom T H 2001 *J. Phys.: Condens. Matter* **13** 10471
[17] Newman D J and Urban W 1975 *Adv. Phys.* **24** 793
[18] Newman D J and Ng B 1989 *Rep. Prog. Phys.* **52** 699
[19] Malovichko G I, Grachev V G and Lukin S N 1986 *Fiz. Tverd. Tela* **28** 991
[20] *Computer Program EPR-NMR* (Department of Chemistry, University of Saskatchewan, Canada)
[21] Newman D J and Siegel E 1976 *J. Phys. C: Solid State Phys.* **9** 4285
[22] Siegel E and Muller K A 1979 *Phys. Rev.* B **19** 109
[23] Donnerberg H, Exner M and Catlow C R A 1993 *Phys. Rev.* B **47** 14
[24] Yeung Y Y 1988 *J. Phys. C: Solid State Phys.* **21** 2453
[25] Agullo-Lopez F and Muller K A 1987 *Cryst. Lattice Defects Amorphous Mater.* **15** 89
[26] Yeom T H, Choh S H, Chang Y M and Rudowicz C 1994 *Phys. Status Solidi* b **185** 417
[27] Waychunas G A 1983 *J. Mater. Sci.* **18** 195
[28] Shuskus A J 1962 *Phys. Rev.* **127** 1529
[29] Muller K A 1958 *Helv. Phys. Acta* **31** 173